

Manipulating atoms in an optical lattice: Fractional fermion number and its optical quantum measurement

J. Ruostekoski,^{1,*} J. Javanainen,^{2,†} and G. V. Dunne^{2,3,4,‡}

¹*School of Mathematics, University of Southampton, Southampton, SO17 1BJ, UK*

²*Department of Physics, University of Connecticut, Storrs, CT 06269, USA*

³*CSSM, Department of Physics, University of Adelaide, SA 5005, Australia*

⁴*Institut für Theoretische Physik, Universität Heidelberg, Philosophenweg 16, 69120 Heidelberg, Germany*

(Dated: October 30, 2021)

We provide a detailed analysis of our previously proposed scheme [Phys. Rev. Lett. **88**, 180401, (2002)] to engineer the profile of the hopping amplitudes for atomic gases in a 1D optical lattice so that the particle number becomes fractional. We consider a constructed system of a dilute two-species gas of fermionic atoms where the two components are coupled via a coherent electromagnetic field with a topologically nontrivial phase profile. We show both analytically and numerically how the resulting atomic Hamiltonian in a prepared dimerized optical lattice with a defect in the pattern of alternating hopping amplitudes exhibits a fractional fermion number. In particular, in the low-energy limit we demonstrate the equivalence of the atomic Hamiltonian to a relativistic Dirac Hamiltonian describing fractionalization in quantum field theory. Expanding on our earlier argument [Phys. Rev. Lett. **91**, 150404 (2003)] we show how the fractional eigenvalues of the particle number operator can be detected via light scattering. In particular, we show how scattering of far-off resonant light can convey information about the counting statistics of the atoms in an optical lattice, including state-selective atom density profiles and atom number fluctuations. Optical detection could provide a truly quantum mechanical measurement of the particle number fractionalization in a dilute atomic gas.

PACS numbers: 03.75.Ss,03.75.Lm,05.30.Pr,11.27.+d

I. INTRODUCTION

Loading alkali-metal atoms into optical lattices has opened up fascinating possibilities to study many-particle systems with a wide range of technology to manipulate the parameters of the system Hamiltonian as well as the quantum states of the atoms. In particular, the flexibility of the experimental preparation of ultra-cold atoms could be an advantage in realizing atomic systems with close analogies to the physical systems, known in other disciplines of modern physics, in which the experimental evidence or theoretical understanding is limited.

We previously proposed a scheme to engineer the spatial profiles of the hopping amplitudes for atoms in an optical lattice [1]. This is achieved by superimposing coherent electromagnetic (em) field amplitudes that induce a coupling between different spin states of the atom and drive transitions between neighboring lattice sites. We considered a particular constructed system of a two-species gas of fermionic atoms in a 1D lattice, where the two components are coupled via an em field with a topologically nontrivial phase profile (with topological properties similar to a soliton, or a phase kink), so that the particle number becomes fractional. In particular, we showed that, in the low energy limit, the resulting

Hamiltonian of the atomic system has a one-to-one correspondence to a relativistic Dirac Hamiltonian describing fractional fermions in quantum field theory [2, 3, 4]. This is related to fractionalization in the polyacetylene polymer systems, where the linearized lattice vibrations are coupled to the electrons so that the dynamics of the electrons is described by a relativistic Dirac equation. We also showed that the fractional part of the particle number in the atomic system can be accurately controlled by modifying the effective detuning of the em field.

Moreover, we proposed an optical measurement scheme for fractional particle number in an atomic gas that could detect directly the fractional eigenvalue and determine atom number fluctuations [5]. In particular, the fractional fermion could be imaged in a phase-contrast set-up, while the atom number fluctuations are reflected in the fluctuations of the number of photons in the light scattered off the lattice.

In this paper we present a detailed description of how fractionalization manifests itself and how it could be optically detected in the atomic regime, using an optically trapped Fermi-Dirac (FD) atomic gas. We show how to engineer spatially inhomogeneous hopping amplitude profile for the atoms in an optical lattice. We extend our analysis in Ref. [1] of different optical and rf/microwave fields to prepare first a dimerized lattice and later to include a discontinuity in the hopping amplitude pattern. We demonstrate both analytically and numerically how the resulting atomic Hamiltonian exhibits a fractional fermion number. We consider different observables, accessible via light scattering experiments, that could di-

*Electronic address: janne@soton.ac.uk

†Electronic address: jj@phys.uconn.edu

‡Electronic address: dunne@phys.uconn.edu

rectly probe the fractional fermion number and its fluctuations.

Adjusting the hopping amplitudes in our scheme in Ref. [1] provided the means of preparing a topologically non-trivial atomic ground state. More recently, similar techniques to engineer the spatial profile of the hopping amplitude between the atoms in adjacent optical lattice sites using em transitions were proposed to create effective magnetic fields in a 2D lattice [6, 7], as well as non-Abelian gauge fields for the atoms in an optical lattice [8]. In Ref. [6] a spatially alternating pattern of hopping amplitudes along one spatial direction was used to induce a non-vanishing phase of particles moving along a closed path on the lattice. Since this phase is proportional to the enclosed area, the hopping amplitude pattern simulates the effects of a magnetic field on charged particles. By introducing a level degeneracy in such a set-up allowed to consider non-Abelian phases for the atoms moving along closed paths [8].

An interesting property of our constructed optical lattice Hamiltonian is that the ultra-cold fermionic atoms exhibit long-wavelength dynamics that is equivalent to relativistic Dirac fermions with a controllable mass and with coupling to a bosonic field. Here the bosonic field is represented by the external em field amplitude inducing the hopping of the atoms between adjacent lattice sites and the mass of the Dirac fermions is proportional to the effective detuning of the coupling field from the resonance. The realizations of emerging relativistic Dirac quasiparticles in condensed matter systems has recently attracted considerable interest, e.g., in graphene systems where the 2D hexagonal lattice structure has low-energy excitations analogous to those of Dirac fermions [9, 10, 11, 12]. The atomic optical lattice systems can be engineered and controlled to a much higher degree than graphene or polymer systems. For instance, the atomic gas could be used to demonstrate the effect of the Dirac fermion mass on the fractional part of the eigenvalue [13] and the finite-temperature contributions to the fractional fermion number in relativistic field theory [14, 15]. The optical lattice could provide a laboratory to simulate the properties of relativistic Dirac fermions also more generally.

Particle number fractionalization is a remarkable phenomenon in both relativistic quantum field theory and condensed matter systems [4, 16]. Jackiw and Rebbi [2, 3] showed that for a fermionic field coupled to a bosonic field with a topologically nontrivial soliton profile, the fermion number can be fractional. The noninteger particle number eigenvalues may be understood in terms of the deformations of the Dirac sea (or the hole sea) due to its interaction with the topologically nontrivial environment. Fractional fermion number has been discussed previously in the condensed matter regime in 1D conjugated polymers (the SSH model) [3, 17, 18]. The existence of fractionally charged excitations in the polymers is typically demonstrated indirectly by detecting the reversed spin-charge relation [18]. The fractional quan-

tum Hall effect (FQHE) can also be explained by invoking quasiparticles, each with a fraction of an electron's charge [19], but the fractionalization mechanism is very different from that in the polymers and in the atomic gas in this paper. The fluctuations of the tunneling current in low-temperature FQHE regime have been measured [20, 21]. Interpreting the current shot noise according to the Johnson-Nyquist formula duly suggests that the current is carried by the fractional Laughlin quasiparticles. Analogous experiments have determined the fractional expectation value of the charge in FQHE in the Coulomb blockade regime [22]. Recently fractional statistics was observed by realizing a quasiparticle interferometer in the FQHE regime [23].

Light scattering can be an efficient probe of quantum statistical properties of ultra-cold atoms. It can provide information about spatial correlation functions between the atoms [24] and spectral properties about excitations [25]. The scattering process could also generate an entanglement between the photons and the many-particle atomic state [26, 27]. In Ref. [5] we adapted the techniques of far off-resonant light scattering in optically thin samples [25] to the atomic gases trapped in optical lattices. In the measurements of the expectation value of the fractional particle number, we make use of the fact that the adjacent lattice sites are occupied by different fermionic species. In a phase-contrast imaging, we may adjust the light scattered from one species to add to the incident beam and the light scattered from the other species to subtract. By measuring the intensity of the scattered light, one may detect the atom number fluctuations in order to demonstrate that not only the expectation value is fractional but also that the fluctuations become vanishingly small. This is required to show that the fractional fermion number represents an eigenstate of a particle number operator. The detection of both the expectation value and the fluctuations would represent a truly quantum mechanical measurement of fractionalization that has been a long-standing challenge in physics. Our proposed measurement techniques could also be useful in detecting fractional Laughlin quasi-particles in rapidly rotating atomic gases [28]. Although the emphasis of our optical detection analysis was on fractionalization, the basic formalism could also be used as a more general optical probing technique of atom number fluctuations in optical lattices. The optical detection of atom number fluctuations in an optical lattice using an analogous approach and the enhancement of the signal by an optical cavity was more recently addressed in Ref. [29, 30].

In addition to providing atomic physics technology for a potentially direct detection of the fractional fermion number and its fluctuations that have so far escaped experimental observation, our dilute atomic gas has a possible advantage, compared to condensed matter systems, in the sense that the atoms form a very clean system: The interatomic interactions are weak and well-understood, the lattice may be prepared without imperfections, and

different parameters of the system Hamiltonian can be controlled.

In Sec. II we introduce the basic optical lattice system to produce a fractional fermion number. In Sec. II A we first explain the lattice Hamiltonian and em-induced atom hopping from site to site, then discuss the nonuniform hopping amplitudes between adjacent lattice sites in a dimerized lattice. Introducing a defect in the regular pattern of hopping amplitudes results in a bound state and a fractional fermion number, localized around the defect; methods to prepare such a defect are also discussed. Pertinent mathematical properties of the fractional fermion number and its fluctuations in a finite lattice are derived in Sec. II B. An example hopping amplitude profile that generates a fractional number $1/3$ is introduced in Sec. III. We show that the long-wavelength limit of the atomic lattice Hamiltonian is equivalent to the relativistic Dirac Hamiltonian in Sec. IV. We review some basic properties of the corresponding Jackiw-Rebbi relativistic model that provides a simple description of the fractionalization process. The optical detection method is explained in Sec. V. We first show how the fractional fermion number could be imaged in a phase-contrast set-up and then how the fluctuations of the fractional observable are reflected in the fluctuations of incoherently scattered light. Finally, a few concluding remarks are made in Sec. VI, where we also address the effects of the harmonic trapping potential.

II. OPTICAL LATTICE SYSTEM

A. Basic physical system

In our scheme to realize particle number fractionalization in atomic gases we consider neutral FD atoms loaded in a periodic 1D optical lattice. The optical potential is induced by means of the ac Stark effect of off-resonant laser beams [31].

Atomic systems in 1D may be created by confining the atoms tightly along the transverse directions. This is typically obtained by means of optical lattices or atom chips. For instance, in recent experiments 1D optical lattices were created from 3D optical lattices by increasing the optical lattice barrier height along two orthogonal directions [32, 33]. This resulted in a 2D array of decoupled 1D tubes of atoms where the atoms in each tube experienced a periodic optical standing wave potential along the axial direction of the tube. If bosonic atoms are confined sufficiently tightly along the two transverse directions, the system approaches the Tonks-Girardeau regime where the impenetrable bosons obey the FD statistics [32].

We analyze an optical lattice system confining two fermionic species using an atomic Hubbard Hamiltonian [34]. In a sufficiently deep lattice each site is assumed to support one mode function (the Wannier function) that is weakly coupled to two nearest neighbor sites. We assume

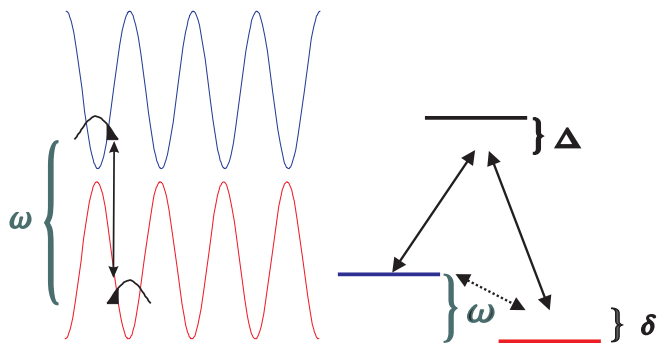


FIG. 1: The energy diagram of the two-species Fermi-Dirac gas in an optical lattice. The atoms occupy two different internal levels and experience different periodic optical potentials shifted by d (on the left). The coupling between the neighboring lattice sites, representing different spin components, is induced by two-photon Raman transitions, or by a superposition of the Raman transition and a one-photon microwave or rf transition (dotted line). The transition region is denoted by the dark shaded area representing the overlap region of the atomic wave functions. The energy difference between the two components in the overlap region is denoted by ω . The two-photon transition is far-detuned by Δ from an intermediate atomic level (on the right), and in this illustration δ stands for the two-photon detuning.

that the hopping of the atoms between adjacent lattice sites only occurs as a result of driving by coherent em fields. This could be realized, e.g., with a FD gas occupying two internal levels $|\uparrow\rangle$ and $|\downarrow\rangle$ that are coherently coupled via an em-induced transition, if the two species experience optical potentials which are shifted relative to each other by d , where $2d$ denotes the lattice period for each state $|\uparrow\rangle$ and $|\downarrow\rangle$; see Fig. 1. The coupling could be a far off-resonant optical Raman transition via an intermediate atomic level, a microwave, or a rf transition. The optical lattice potential with alternating spin states in alternating sites may be realized, e.g., by combining σ^+ and σ^- polarized lasers [35], or when the light beam is blue-detuned from an internal transition of the atoms in level $|\uparrow\rangle$ and red-detuned from a transition in level $|\downarrow\rangle$. A simple example 1D lattice potential in that case is $V_{\uparrow}(x) = V_0 \sin^2(\pi x/2d)$, and $V_{\downarrow}(x) = -V_0 \sin^2(\pi x/2d)$.

In our example set-up of Fig. 1, the neighboring lattice sites represent atoms in different internal levels and are separated by a distance d . Here $d = \lambda/[4 \sin(\theta/2)]$ is obtained by two laser beams, with the wavelength λ , intersecting at an angle θ . The lattice spacing can be easily modified by changing the angle between the lasers. We may write the annihilation operators for fermionic atoms as $c_{2k+1,\uparrow}$ and $c_{2k,\downarrow}$ at odd and even numbered lattice sites, occupying the internal levels \uparrow and \downarrow , respectively. In the following we suppress the explicit reference to the different internal levels and write the annihilation operator for the atoms in the k th site simply as c_k . The

Hamiltonian for the atomic system then reads

$$\frac{H}{\hbar} = \sum_k \left[\epsilon_k c_k^\dagger c_k - (\kappa_k c_{k+1}^\dagger c_k + \kappa_k^* c_k^\dagger c_{k+1}) \right]. \quad (1)$$

The em-induced coupling between the two internal states between the k th and the $(k+1)$ th site is described by

$$\kappa_k = \int d^3r \psi_\sigma^*(\mathbf{r} - \mathbf{r}_k) \Omega(\mathbf{r}) \psi_{-\sigma}(\mathbf{r} - \mathbf{r}_{k+1}), \quad (2)$$

and ϵ_k stands for the effective detuning and/or external potential variation between different sites. The em-coupling terms are the analogues of the hopping terms in the corresponding polymer Hamiltonian [3]. The mode functions of the individual lattice sites (Wannier functions) are denoted by $\psi_\sigma(\mathbf{r} - \mathbf{r}_i)$, with $\sigma = \uparrow, \downarrow$ and $-\sigma = \downarrow, \uparrow$, respectively. We assume that the em coupling between the internal levels $\Omega(\mathbf{r})$ is the only transition mechanism for the atoms between neighboring lattice sites, and therefore ignore the direct tunneling. $\Omega(\mathbf{r})$ could, for instance, be an effective two-photon Rabi frequency at the position \mathbf{r} . In this respect our optical-lattice scheme is closely related to the microtrap scheme discussed recently as a method of transporting atoms for the purposes of quantum information processing [36]. We neglect the s -wave scattering between the two FD species. This process can be made weak by having a small spatial overlap between the mode functions of the adjacent lattice sites.

Even though the optical lattice may be part of a larger trap, which could generate interesting physics in its own right, we simplify by setting $\epsilon_k = (-1)^k \delta/2$ to be constant along the lattice separately for the even (\downarrow) and for the odd (\uparrow) sites that are split by the energy difference δ . We mostly concentrate on the simplest case $\delta = 0$. The fractional fermion number arises from certain types of defects in the couplings κ_k . In this paper we illustrate by concentrating on one such set-up; we consider a *dimerized* lattice generated by the coupling matrix element that alternates from site to site between two values $a + \mu$ and $a - \mu$, except that at the center of the lattice there is a defect such that the same coupling matrix element appears twice. In the following, we use the notation introduced in Ref. [5, 37].

1. Dimerized optical lattice

In this section we introduce an alternating pattern in the atomic hopping amplitudes. This establishes a dimerized optical lattice. If we also add a defect in the pattern of alternating coupling matrix elements, this results in a fractional fermion number, localized around the defect. This type of schemes are the subject of the following two sections.

We consider the coupling frequency $\Omega(\mathbf{r})$ to be a phase-coherent superposition of two field amplitudes:

$$\Omega(\mathbf{r}) = \mathcal{V}(\mathbf{r}) + \mathcal{U}(\mathbf{r}) \sin\left(\frac{\pi x}{d}\right). \quad (3)$$

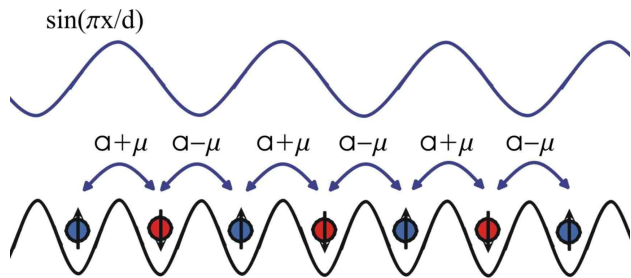


FIG. 2: Dimerized optical lattice with spatially alternating hopping amplitude for atoms between adjacent lattice sites. The hopping is induced by electromagnetic field (as in Fig. 1) whose amplitude varies according to Eqs. (3) and (6). Here a_k and μ_k are assumed to be constant along the lattice. The coefficient in the front of μ is determined by the value of $\sin(\pi x/d)$ at the middle between the lattice sites where the Wannier functions of the two lattice sites overlap.

We can assume that the matrix elements

$$a_k \equiv \int d^3r \psi_\sigma^*(\mathbf{r} - \mathbf{r}_k) \mathcal{V}(\mathbf{r}) \psi_{-\sigma}(\mathbf{r} - \mathbf{r}_{k+1}), \quad (4)$$

$$\mu_k \equiv \int d^3r \psi_\sigma^*(\mathbf{r} - \mathbf{r}_k) \mathcal{U}(\mathbf{r}) \psi_{-\sigma}(\mathbf{r} - \mathbf{r}_{k+1}), \quad (5)$$

do not change sign over the length of the lattice. The purpose of the standing wave in Eq. (3) is to introduce a spatially alternating sign for the hopping amplitude along the lattice.

We assume that $\sin(\pi x/d)$ in Eq. (3) is approximately constant over the small spatial overlap area of two neighboring lattice site atom wavefunctions. One of the lattice sites has the potential minimum at $x = 0$ and its two nearest neighbor sites minima at $x = \pm d$. The spatial overlap of the atomic wavefunctions centered at the sites $x = 0$ and $x = \pm d$ has the maximum at $x = \pm d/2$. The $\sin(\pi x/d)$ term in the hopping amplitude in the overlap region at $x = d/2$ is equal to one and at $x = -d/2$ it is equal to -1 . With similar arguments it is easy to see that the hopping amplitude alternates between the values ± 1 at each overlap area and we obtain (see Fig. 2)

$$\kappa_k \simeq a_k + (-1)^k \mu_k. \quad (6)$$

In this approximation, we take a_k and μ_k real and in the actual calculations assume them to be constant along the lattice, $a_k = a$ and $\mu_k = \mu$.

The field amplitude, Eq. (3), required to generate the hopping amplitude, Eq. (6), represents a phase-coherent superposition of a standing wave and a field amplitude with a uniform phase profile. The field superposition could be produced, e.g., by using optical holograms. We will address such techniques in more detail in the next section, when we consider a more complicated field profile needed to prepare fractional fermions. Due to the relatively simple form of Eq. (3), the field configuration could be generated by superposing an optical standing wave and a rf, microwave, or an optical field \mathcal{V} . The two fields both need to couple the states $|\uparrow\rangle$ and $|\downarrow\rangle$, or to

form part of a multi-level, multi-photon transition that couples the two states together.

The standing wave in the hopping amplitude has the period $2d$ when the period of the amplitude of the lattice lasers forming the optical potential is equal to $4d$. The different periodicity may be obtained by using a different angle θ' between two counter-propagating lasers, so that $d = \lambda'/[2\sin(\theta'/2)]$, where λ' is the wavelength of the $\sin(\pi x/d)$ hopping field.

Alternatively, the $\sin(\pi x/d)$ hopping term may be prepared by using the same wavelength $\lambda' = \lambda$ and intersection angle $\theta' = \theta$ as in the optical lattice potential with a two-photon optical Raman transition (Fig. 1). The strength of an off-resonant two-photon Rabi frequency in the limit of large detuning, Δ , from the intermediate state is $\Omega \propto \mathcal{R}_1\mathcal{R}_2/\Delta$, where \mathcal{R}_i denote the Rabi frequencies in the individual transitions [25]. For two standing-wave one-photon couplings displaced from one another by d , the two-photon Rabi frequency is $\Omega \propto \sin(\pi x/2d) \cos(\pi x/2d) \propto \sin(\pi x/d)$, so, even though the period of the lattice laser amplitude is $4d$, the effective field amplitude of the two-photon transition has the desired period $2d$.

In order to understand the effect of dimerization, we follow [17] and consider the Hamiltonian (1) for the uniform lattice $\epsilon_k = 0$ with the coupling (6) in the case of periodic boundary conditions. The adjacent lattice sites are separated by d and we can obtain the reduced zone representation for $-\pi/2d < p \leq \pi/2d$ by transforming the lattice operators according to

$$c_{p-} = \frac{1}{\sqrt{N}} \sum_k e^{ipkd} c_k, \quad (7)$$

$$c_{p+} = \frac{1}{\sqrt{N}} \sum_k e^{ipkd} (-1)^k c_k. \quad (8)$$

In terms of the valence and the conduction band operators of the undimerized system, c_{p-} and c_{p+} , the Hamiltonian (1) reads:

$$\frac{H}{\hbar} = \sum_p [e_p(c_{p+}^\dagger c_{p+} - c_{p-}^\dagger c_{p-}) + \Delta_p(c_{p+}^\dagger c_{p-} + c_{p-}^\dagger c_{p+})], \quad (9)$$

with

$$\Delta_p \equiv 2\mu \sin(pd), \quad e_p \equiv 2a \cos(pd). \quad (10)$$

This can be diagonalized by the Bogoliubov transformation

$$b_{p-} = \alpha_p c_{p-} - \beta_p c_{p+}, \quad (11)$$

$$b_{p+} = \alpha_p c_{p+} + \beta_p c_{p-}, \quad (12)$$

with the appropriate choice of the coefficients α_p and β_p , so that

$$\frac{H}{\hbar} = \sum_p E_p (b_{p+}^\dagger b_{p+} - b_{p-}^\dagger b_{p-}). \quad (13)$$

The quasiparticle energies are given by

$$E_p \equiv \sqrt{e_p^2 + \Delta_p^2}, \quad (14)$$

and the spectrum exhibits an energy gap equal to $4\hbar|\mu|$ at the reduced zone boundary $p = \pm\pi/2d$, due to the dimerization field. We may define the atomic correlation length according to Eq. (14), analogously to the BCS theory:

$$\xi \simeq \left| \frac{e'(p_F)}{\Delta(p_F)} \right| = \left| \frac{ad}{\mu} \right|, \quad (15)$$

where $p_F = \pi/2d$ is the Fermi momentum.

2. Defect in the pattern of alternating hopping amplitudes

In this section we construct a field amplitude that breaks the symmetry of the dimerized lattice formed by the alternating pattern of the hopping amplitudes. This is obtained by generating a defect at the center of the lattice, so that the same coupling term between the lattice sites appears twice in a row.

For an even number of sites, or in the limit of an infinite lattice, the two hopping amplitude profiles

$$\kappa_k = a \pm (-1)^k \mu, \quad (16)$$

yield ground states with equal energies. We may join these two field configurations at the center of the lattice by synthesizing a defect in the alternation pattern in such a way that the left side of the lattice represents the lower sign of the hopping term (16) and the right side of the lattice the upper sign; see Fig. 3. The em field required to induce the desired coupling may be written in the following form:

$$\Omega(\mathbf{r}) = \mathcal{V}(\mathbf{r}) + \mathcal{U}(\mathbf{r})\varphi(x) \sin\left(\frac{\pi x}{d}\right), \quad (17)$$

where the field $\varphi(x)$, satisfying $\varphi(h) = -\varphi(-h) = 1$ for all $h \gg d$, exhibits a spatial profile of a soliton, or a phase kink. Here $\varphi(x)$ has a phase jump of π at $x = 0$, representing a topological phase singularity. The corresponding hopping amplitude reads

$$\kappa_k = a + \varphi_k (-1)^k \mu, \quad (18)$$

where $\varphi_k = \varphi(x_k)$; see Fig. 3.

This type of a coupling represents a superposition of a field with a constant phase profile \mathcal{V} (producing a) and the field $\varphi(x)\sin(\pi x/d)$. The entire field configuration (17) could be prepared optically by synthesizing multi-beam superposition states using diffractive optical components. In particular, computer-generated holograms and spatial light modulators can act as optical phase holograms to shape laser fields in order to generate a sharp phase kink $\varphi(x) \sim x/|x|$, combined with the sine

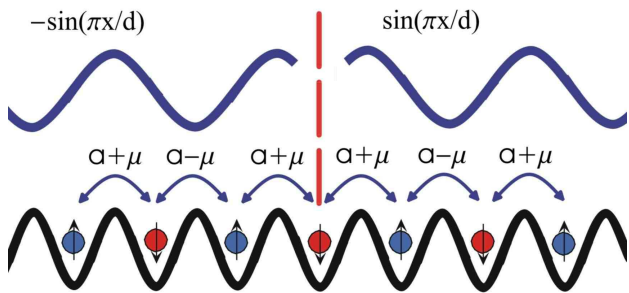


FIG. 3: Defect in the pattern of alternating hopping amplitudes. The coefficient in the front of μ is determined by the product $\varphi(x) \sin(\pi x/d)$ at the middle between the lattice sites where the Wannier functions of the two lattice sites overlap. The soliton, or a kink, profile of $\varphi(x)$ generates a defect in the hopping amplitude pattern, so that the same coupling matrix element appears twice. The defect is marked by a dashed (red) vertical line. Here $\varphi(x) \sim x/|x|$.

wave and the field \mathcal{V} . The holograms are typically calculated by specific algorithms that optimize the phase and/or intensity profiles of the field according to the merit function criteria. Optical holography has been experimentally used to prepare phase singularities on light beams [38] and has been proposed as an efficient tool for phase imprinting topological defects in atomic Bose-Einstein condensates [39, 40].

Alternatively, one may generate the effective coupling field, Eq. (17), by superposing two different transition paths between the states $|\uparrow\rangle$ and $|\downarrow\rangle$. One of the transition paths, that may involve a multi-photon transition via intermediate levels or a single-photon transition with no intermediate levels, produces an effective Rabi frequency with a uniform phase profile, representing the field \mathcal{V} in Eq. (17) and a in Eq. (18). The other transition path generates the field $\varphi(x) \sin(\pi x/d)$. This could be obtained, e.g., with a two-photon transition via an intermediate level, so that the first transition is driven by $\varphi(x)$ and this is followed by the second one driven by $\sin(\pi x/d)$; see Fig. 4.

The effective $\varphi(x)$ field might be produced either by making use of the (rf or microwave) transition between the spin states, or by means of an optical transition other than the one used to produce the $\sin(\pi x/d)$ standing wave. In our studies of fractionalization, the precise form of the field $\varphi(x)$ is not very crucial, as the relevant physics depends on its asymptotic, topological behavior. A phase profile with topological properties similar to $\varphi(x)$ could be prepared, e.g., by means of a standing em wave $\sin(qx)$ satisfying $q \ll \pi/d$. The period of $\sin(qx)$ needs to be chosen long so that along the lattice there is only one node point located near the center of the lattice. Such a 1D standing wave could be obtained using microwaves or, alternatively, optical fields if the intersection angle between the two laser beams could be chosen such that $\sin(\theta/2) \ll \lambda/2d$, where λ is the laser wavelength. In Ref. [1] we proposed also other potential experimental schemes to prepare the hopping field based on em field

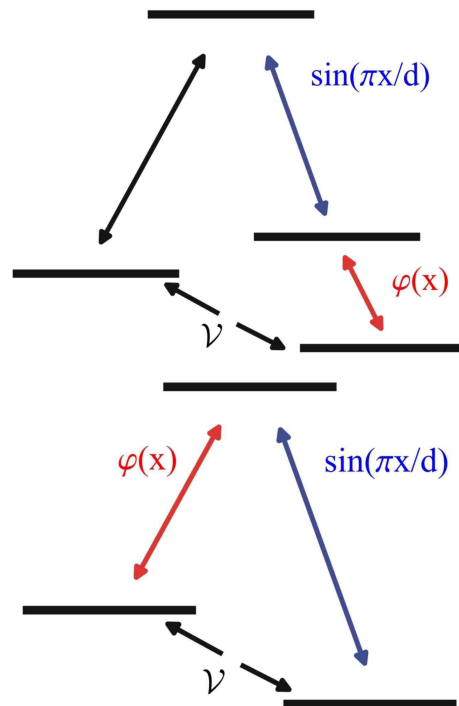


FIG. 4: Examples of the field configurations that are not based on an optical hologram and that can generate the field amplitude in Eq. (17). Two different transition paths synthesize the superposition between \mathcal{V} and $\varphi(x) \sin(\pi x/d)$. The field profile $\varphi(x) \sin(\pi x/d)$ is produced by two successive transitions, so that the effective Rabi frequency is the product of $\varphi(x)$ and $\sin(\pi x/d)$. On top, a far-detuned microwave or rf field, generating $\varphi(x)$, is combined with an optical Raman two-photon transition via a far-detuned electronically excited intermediate level, where one of the transitions is driven by the standing wave $\sin(\pi x/d)$. The effective Rabi frequency for the corresponding three-photon transition is proportional to $\propto \varphi(x) \sin(\pi x/d)$. On bottom, an optical Raman two-photon transition where one transition is driven by $\varphi(x)$ and the other one by $\sin(\pi x/d)$.

couplings.

3. Alternative scheme based on field gradients

The scheme introduced in Ref. [1] to prepare a nonuniform hopping amplitude pattern for the atoms in an optical lattice has an alternative proposed realization by Jaksch and Zoller [6]. In Ref. [6] a spatially alternating pattern of hopping amplitudes was generated in a 2D lattice along one spatial direction in order to induce a nonvanishing phase on atoms moving along a closed path in the lattice, therefore simulating the effect of a magnetic field on electrons. This approach uses field gradients combined with an em-induced coupling. In the following we adapt the basic scheme of Ref. [6] to our fractionalization study.

As in the previous section, we assume that the hopping

of the atoms between adjacent lattice sites is driven by em fields. To be specific, let us think of two-photon transitions in the Raman configuration with a far-off resonant intermediate state. This setup is functionally equivalent to transitions in an effective two level system with the transition frequency ω equal to the difference of the energies of the states \uparrow and \downarrow , driven by a field whose effective frequency is the frequency difference between the two laser frequencies. In Fig. 5(a) we draw the scheme of transitions from site to site. The horizontal lines represent the energies of the levels \uparrow and \downarrow , alternating between adjacent sites, and resonant transitions between the levels at the effective frequency of the driving field ω are marked with arrows. In this basic lattice the site-to-site couplings are the same.

Next assume that in some manner a potential has been added to the atoms that grows linearly along the lattice. Correspondingly, the Hamiltonian picks up an additional term

$$H_s = \xi \sum_{j=-N_h}^{N_h} j c_j^\dagger c_j. \quad (19)$$

For notational simplicity the lattice sites are numbered from $-N_h$ to N_h . We specifically pick $\xi = \hbar\omega$, and imagine tuning the fields driving the transitions to the effective frequency 2ω . As demonstrated in Fig. 5(b), in this way every second transition is on resonance. On the other hand, every second transition now has the effective resonance frequency 0, and the field with the frequency 2ω assumedly becomes ineffective at transferring atoms in such transitions. To compensate, let us add light fields to make the effective frequency 0 to drive the transition between the sites that the potential Eq. (19) decoupled, as in Fig. 5(c). Resonant couplings between all adjacent sites have now been established. To prepare for the final step of the argument, in Fig. 5(c) we have also indicated a few possible transitions without a resonant final level. As we denote symbolically by using solid-line and dashed-line arrows for the driving fields, the coupling coefficients for the alternating transitions need not be equal. At this stage we have a dimerized lattice.

In the last step we modify the added potential to make the corresponding force change sign at the center of the lattice, so that

$$H_s = \xi \sum_{j=-N_h}^{N_h} |j| c_j^\dagger c_j \quad (20)$$

replaces Eq. (19). Figure. 5(d) shows both the level scheme for the newly adjusted lattice potential, and the possible transitions. This time around two solid-arrow transition in a row are on resonance at the center, so that we have established a defect in the couplings precisely as needed to prepare a half-fermion.

The technical issue with these ideas is to set up the piecewise linear potentials. A potential of the type Eq. (19) could be generated, say, with a magnetic

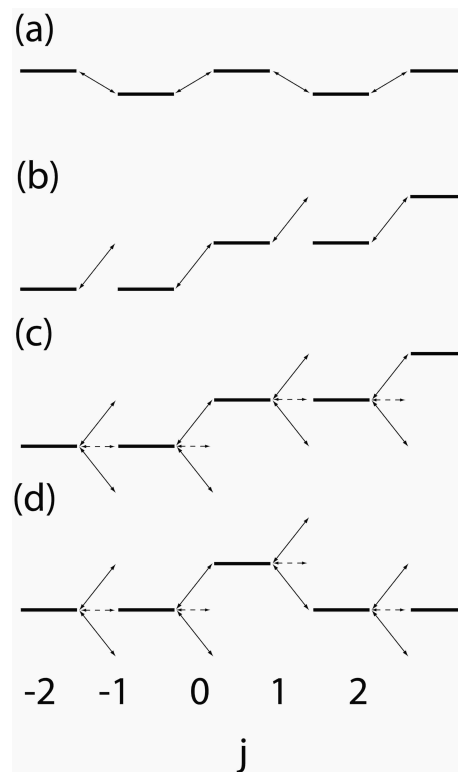


FIG. 5: A scheme for a dimerized lattice based on the interplay between internal and center-of-mass energies of the atoms. (a) The energies of the relevant internal states (\uparrow and \downarrow) of an atom at lattice sites $j = -2, \dots, 2$ are marked by horizontal bars, with resonant transitions between the states displayed by solid arrows. (b) After a constant energy difference between adjacent lattice sites is added to the atoms, for a given set of driving fields only half of the transitions can be on resonance. (c) Another set of lasers frequencies is added, which render also the remaining transitions resonant (dashed arrows). A dimerized lattice has been prepared. Several transitions without a resonant final state are also indicated. (d) In a variation of the scheme in part (b), a constant energy difference is added between every state pair to the left of $j = 0$, and the negative of the same energy difference between state pairs to the right of $j = 0$. The same coupling as in part (c) now realize a dimerized lattice with a defect.

field ramp that shifts Zeeman levels, using ac stark shifts due to added off-resonant laser or microwave fields, in the case of polar molecules static electric fields, or even by accelerating the optical lattice. The reversal of the force at the center of the lattice in Eq. (20) could, e.g., in the case of off-resonant lasers be prepared using optical holograms or spatial light modulators. The required field gradients may also be generated by shining a laser through an absorption plate with a linearly changing optical thickness.

4. Remarks

We have demonstrated how em field-induced hopping of atoms between adjacent lattice sites can be a very useful tool in engineering a rich variety of atomic lattice Hamiltonians. A nonuniform field amplitude, with a periodic spatial profile, is sufficient to prepare a dimerized lattice. One may also introduce a defect in the regular pattern of hopping amplitudes. We will next show that the hopping amplitude profile with such a defect in the pattern of alternating coupling matrix elements results in a bound state and a fractional fermion number, localized around the defect. Such a coupling frequency also converts the atomic lattice Hamiltonian (1) in the continuum limit into the Dirac Hamiltonian exhibiting fractional particle number in relativistic field theory.

B. Fractional fermion in a finite lattice

In this Section we consider the Hamiltonian (1) in the presence of the hopping field with a defect, Eq. (18), along the lines of Ref. [42], for a finite lattice and without a continuum limit. We use hard-wall boundary conditions, i.e., the lattice simply terminates at the edges as if the first sites past the ones included in the lattice were forced to be empty. We demonstrate how a lump with the particle number expectation value of a half emerges on top of the a homogeneous background fermion density. We also discuss numerical techniques used to study the fractional fermion, both as it comes to the expectation value and the fluctuations of the atom number, and present representative examples.

1. Elementary half-fermion

Suppose we can find fermion operators γ_n of the form

$$\gamma_p = \sum_k U_{kp} c_k = \sum_k a_k c_k \quad (21)$$

such that the Hamiltonian (1) becomes

$$\frac{H}{\hbar} = \sum_p \omega_p \gamma_p^\dagger \gamma_p, \quad (22)$$

then we have diagonalized the Hamiltonian. Any one of the operators γ_p , call it γ , should then satisfy

$$\left[\gamma, \frac{H}{\hbar} \right] = \omega \gamma. \quad (23)$$

It follows readily from Eqs. (21)–(23) that the column vectors a_k of the matrix U_{kp} are the orthonormal eigenvectors of the eigenvalue problem

$$(\epsilon_k - \omega) a_k - \kappa_k a_{k+1} - \kappa_{k-1} a_{k-1} = 0, \quad (24)$$

which also yields the corresponding eigenvalues ω_p . As in Eq. (24), the couplings κ_k may be assumed real without a loss of generality, and so we take the matrix U to be real and orthogonal

$$U_{kp}^{-1} = U_{pk}. \quad (25)$$

We consider a sharp defect $\varphi(x) \sim x/|x|$ in the hopping amplitude profile. As in Ref. [42], we take the number of lattice sites to be $N_s \equiv 2N_h + 1 \equiv 4n + 1$, where n itself is an integer, and number the sites with integers ranging from $-N_h$ to N_h . For illustration, pick $n = 2$, use an x to denote a lattice site, and \pm the couplings $a \pm \mu$, then our lattice with the couplings reads

$$x - x + x - x + x + x - x + x - x \quad (26)$$

The defect in the middle, two consecutive plus signs, is the crux of the matter.

We assume here a uniform lattice with the effective energy splitting between the adjacent sites $\delta = 0$, so that $\epsilon_k \equiv 0$. It is easy to see from the structure of Eq. (24) that if ω is an eigenvalue, then so is $-\omega$ (the conjugation symmetry); and the eigenvectors transform into one another by inverting the sign of every second component. We will label the eigenvectors as $-N_h \dots N_h$ in ascending order of frequency, and assign the labels $\pm p$ to such \pm pair of states. Correspondingly, the transformation matrix U satisfies

$$|U_{kp}| = |U_{k,-p}|. \quad (27)$$

But under our assumptions, the number of eigenvalues and eigenstates is odd. The \pm symmetry implies that an odd number of the eigenvalues must equal zero. Except for special values of the couplings a and μ , there is one zero eigenvalue. We call the corresponding eigenstate the zero state. Provided a and μ have the opposite signs and $|a| > |\mu|$, all odd components in the zero state equal zero and the even components are of the form [37]

$$x_k = x_0 \left(-\frac{a + \mu}{a - \mu} \right)^{|k|/2}. \quad (28)$$

The normalizable zero state becomes the narrower, the closer in absolute value a and μ are. For a broadly distributed bound mode, $|a| \gg |\mu|$, we obtain from Eq. (28) the limit

$$\frac{x_k}{x_0} \simeq (-1)^{|k|/2} \exp(-|x_k - x_0|/\xi), \quad (29)$$

where ξ is the atomic correlation length calculated in Eq. (15). Since the size of the zero state depends on the relative strength of the superposed electromagnetic fields via the correlation length, it could be varied experimentally. This is different from the polymer case, where the size of the bound state is fixed.

Suppose next that the system is at zero temperature, and contains $N_f = N_h + 1$ fermions. The exact eigenstates p at the ground state are then filled up to zero state

and empty at higher energies, with occupation numbers $n_p = 0$ or 1, where

$$n_p \equiv \langle \gamma_p^\dagger \gamma_p \rangle. \quad (30)$$

The number operator for the fermions at site k correspondingly reads from Eqs. (21) and (25)

$$c_k^\dagger c_k = \sum_{pq} U_{kp} U_{kq} \gamma_p^\dagger \gamma_q, \quad (31)$$

so that the expectation value of the fermion number at the site k is

$$\begin{aligned} \langle c_k^\dagger c_k \rangle &= \sum_{p=-N_h}^0 |U_{kp}|^2 = \sum_{p=-N_h}^{-1} |U_{kp}|^2 + |U_{k0}|^2 \\ &= \frac{1}{2} \sum_{p=-N_h}^{-1} |U_{kp}|^2 + \frac{1}{2} \sum_{p=+1}^{N_h} |U_{kp}|^2 + |U_{k0}|^2. \end{aligned} \quad (32)$$

Here we have explicitly separated the zero state and used the symmetry $|U_{kp}| = |U_{k,-p}|$. The matrix U_{kp} defines a complete basis and we can use the corresponding orthogonality of U by combining the first two terms and one-half of the third term on the last line of Eq. (32):

$$\langle c_k^\dagger c_k \rangle = \frac{1}{2} \sum_{p=-N_h}^{N_h} |U_{kp}|^2 + \frac{1}{2} |U_{k0}|^2 = \frac{1}{2} + \frac{1}{2} |U_{k0}|^2. \quad (33)$$

By virtue of the same orthogonality, localized with the zero state there is a lump with $\frac{1}{2} \sum_k |U_{k0}|^2 = \frac{1}{2}$ fermions on top of a uniform background of half a fermion per site.

This lump is the celebrated half of a fermion [2, 3, 4]. It is the result of adding a fermion to the zero state which has a nonvanishing occupation probability only for every second site. Therefore the half-fermion rising from the constant background resides on every second lattice site, here on the even-numbered sites. For the remaining lattice sites the mean occupation number is exactly a half.

As a result of the defect the normalizable zero state is localized around the phase kink. This zero state creates a fractional deficit of states in the valence and the conduction bands, as can be observed in Eq. (32). In the presence of the conjugation symmetry, the density of states is a symmetric function of the energy, and both bands have locally a deficit of one-half of a state.

2. Fermion numbers and their fluctuations

To demonstrate the precise meaning of the fractional fermion, we define two smoothed fermion number operators using an envelope function α_k that covers the zero state around the phase kink;

$$\hat{N} = \sum_k \alpha_k c_k^\dagger c_k, \quad \tilde{N} = \sum_k \alpha_k \left(c_k^\dagger c_k - \frac{1}{2} \right). \quad (34)$$

The idea is that an experiment with a limited resolution may be expected to address many lattice sites at once. Although the numbers α_k are real in all of our worked-out examples, for maximum flexibility we allow them to be complex. The difference between the operators \hat{N} and \tilde{N} is that in the latter we have subtracted the constant background fermion number $\frac{1}{2}$ at each lattice site.

Let us so far assume that the numbers α_k vary little from site to site, and that their values in a region that covers the half-fermion lump is well approximated by unity. We then have from Eq. (33)

$$\langle \tilde{N} \rangle = \frac{1}{2} \sum_k \alpha_k |U_{k0}|^2 = \frac{1}{2}, \quad (35)$$

which just reiterates the observation that the lump contains, on the average, half of a fermion above the uniform background.

There is more to a fractional fermion number, however, than the average density. So far we have only dealt with the *expectation* values of the atom numbers. However, the *fluctuations* can be small as well, indicating that the half-fermion represents an eigenstate of the operator \tilde{N} [42, 43]. Since the fluctuations are the same for the operators \hat{N} and \tilde{N} , we focus on the former. The expectation value of \hat{N} is

$$\begin{aligned} \langle \hat{N} \rangle &= \sum_k \alpha_k \langle c_k^\dagger c_k \rangle \\ &= \sum_k \alpha_k U_{kp} U_{kq} \langle \gamma_p^\dagger \gamma_q \rangle \\ &= \sum_k \alpha_k U_{kp}^2 n_p, \end{aligned} \quad (36)$$

and for the square we have

$$\begin{aligned} \langle \hat{N}^\dagger \hat{N} \rangle &= \sum_{kl} \alpha_k^* \alpha_l \langle c_k^\dagger c_k c_l^\dagger c_l \rangle \\ &= \sum_{klpqrs} \alpha_k^* \alpha_l U_{kp} U_{kq} U_{lr} U_{ls} \langle \gamma_p^\dagger \gamma_q \gamma_r^\dagger \gamma_s \rangle \\ &= \sum_{klpq} \alpha_k^* \alpha_l [U_{kp}^2 U_{lq}^2 n_p n_q + U_{kp} U_{kq} U_{lp} U_{lq} (n_p - n_p n_q)] \\ &= |\langle \hat{N} \rangle|^2 + (\Delta N)^2, \end{aligned} \quad (37)$$

where the part characterizing the fluctuations is

$$\begin{aligned} (\Delta N)^2 &= \langle \hat{N}^\dagger \hat{N} \rangle - |\langle \hat{N} \rangle|^2 \\ &= \sum_{klpq} \alpha_k^* \alpha_l U_{kp} U_{kq} U_{lp} U_{lq} n_p (1 - n_q). \end{aligned} \quad (38)$$

Although we always use the zero-temperature Fermi sea with the occupation numbers $n_p = 0$ or 1 for the γ_p fermions in our explicit examples, this assumption has not been used in the analysis of the fluctuations. With the appropriate thermal occupation numbers n_p , expressions such as Eq. (38) apply also at finite temperature [14, 15].

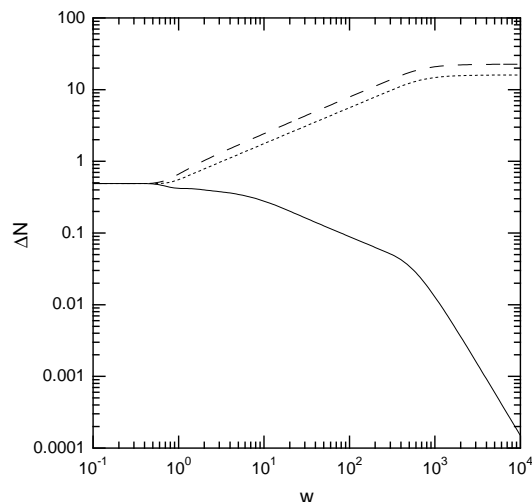


FIG. 6: Coherent atom number fluctuations ΔN under a Gaussian (solid line) and alternating-sign Gaussian (dashed line) envelopes, α_k^G and α_k^A , and the corresponding incoherent atom number fluctuations $(\Delta N)_i$ (dotted line) as a function of the width of the Gaussian w . The lattice parameters are $N_s = 1025$, $N_f = 513$, and $\mu = -0.1 a$.

For illustration we use the Gaussian shape,

$$\alpha_k^G = e^{-(k/w)^2}. \quad (39)$$

We take a lattice with $N_s = 1025$ sites, pick the parameters $\mu = -0.1 a$, put in $N_f = 513$ fermions so that the zero state is the last filled state, and find the rms fluctuations of the fermion number ΔN as a function of the width of the weight function w . The result is shown as the solid line on a log-log plot in Fig. 6. The notch around $w = 1$ indicates that at this point the weight factors α_k start to span several lattice sites. Another break in the curve is seen at about $w = 10$ when the weight function covers the whole zero state. Thereafter the fluctuations behave as $\Delta N \propto w^{-1/2}$. The fermion number \hat{N} under the weight function becomes more sharply defined as the region for averaging grows broader. Finally, at $w \sim 500$, the weights α_k effectively cover the entire lattice. The fluctuations then decrease even faster with increasing w , as is appropriate for the fixed fermion number in the lattice as a whole.

Let us next suppose that the weights α_k can be arranged to alternate in sign from site to site. Specifically, we use

$$\alpha_k^A = (-1)^k e^{-(k/w)^2}. \quad (40)$$

Since the half-fermion is confined entirely to the even-numbered sites, this weight has the effect that in the limit $w \rightarrow \infty$ the constant background is automatically subtracted as far as mean atom numbers go; $\langle \hat{N} \rangle = \langle \tilde{N} \rangle = \frac{1}{2}$. Regarding fluctuations, we again use Eq. (38). The resulting ΔN is plotted in Fig. 6 as a function of the width w as the dashed line for the same problem parameters that were used for the single-sign Gaussian α_k^G . Once

the envelope covers several sites, the fluctuations for the models α_k^G and α_k^A go separate ways, and in the latter case actually increase with increasing width w until the whole lattice is covered.

Our final case of fluctuations is the case of simply adding the particle number fluctuation at each site with the weights $|\alpha_k|^2$, as if the fluctuations were independent. We thus have the “incoherent” fluctuations,

$$\begin{aligned} (\Delta N)_i^2 &= \sum_k |\alpha_k|^2 \left(\langle c_k^\dagger c_k \rangle - \langle c_k^\dagger \rangle \langle c_k \rangle \right) \\ &= \sum_{kpq} |\alpha_k|^2 U_{kp}^2 U_{kq}^2 n_p (1 - n_q). \end{aligned} \quad (41)$$

This is what becomes of the “coherent” fluctuations of Eq. (38) if only the diagonal terms with $k = l$ are kept. A physical motivation for such a rule could be that the coefficients α_k are uncorrelated random numbers (with zero mean).

The incoherent fluctuations $(\Delta N)_i$ are plotted in Fig. 6 as a dotted line along with the coherent fluctuations for the two envelopes α_k^G and α_k^A ; which envelope is used in the incoherent case does not matter. The magnitude of the incoherent fluctuations is between the magnitudes of the fluctuations for the two coherent cases. As soon as the widths of the Gaussians are sufficient to cover several lattice sites, the coherent fluctuations for the alternating-sign Gaussian α_k^A are about a factor of $\sqrt{2}$ times the incoherent fluctuations.

In the standard half-integer fermion number argument one uses a smooth envelope such as α_k^G and subtracts a non-fluctuating neutralizing background of $\frac{1}{2}$ charge per lattice site, whereupon $\langle \tilde{N} \rangle \rightarrow \frac{1}{2}$ and $\Delta N \rightarrow 0$ with an increasing envelope width w . The intermediate regime that occurs once the zero state is covered is the crux of the matter. Not only does the expectation value of fermion number \tilde{N} equal $\frac{1}{2}$, but the fluctuations are small and \tilde{N} therefore has an eigenvalue $\frac{1}{2}$.

A perusal of the dotted line for the incoherent fluctuations in Fig. 6 qualitatively suggests that the fluctuations of the fermion number at each individual site are comparable to what one would expect if each site simply had the fermion number of either 0 or 1 with the equal probabilities of $\frac{1}{2}$. On the other hand, the atom number fluctuations appear to be anticorrelated between adjacent sites. Thus, if one sums up the atom numbers with a weight that has a sign alternating from site to site (dashed line), the resulting fluctuations in the summed atom number are larger than they would be for uncorrelated fluctuations. Also, if one sums over the atom numbers with a weight that varies little from site to site (solid line), such anticorrelated fluctuations tend to cancel in the sum. In short, anticorrelations of atom number fluctuations between neighboring sites undoubtedly contribute to the impression of a sharp eigenvalue for a smoothly weighted sum of occupation number operators. The role of longer-range correlations (next-nearest sites, etc.) deserves further study, but it will not be undertaken

here.

3. Variations of the half-fermion

The main point to emphasize about the derivation of Eq. (33) is that the fractional particle number is the property of the system as a whole. Adding the last fermion that occupies the zero state adds one particle, but makes a soliton containing half of a fermion. This means that before the addition there was a hole in the density distribution with half of a fermion missing, an observation easily verified by a calculation similar to the one that lead to Eq. (33). The hole clearly depends on the shapes of the wave functions and on the occupation numbers of the non-zero states, hence so does the half-integer fermion number.

Fractionalization is a robust phenomenon. Something akin to a localized zero state occurs as soon as the regular alternation of the couplings between adjacent states gets out of rhythm around a defect. In particular, the defect does not have to be confined to one lattice site; this should make the experiments easier. Moreover, a spike with about half a fermion standing above the background may be seen when the particle number deviates from $(N_s + 1)/2$ by, say, ten per cent; and a hole of about half a fermion may similarly persist even if the particle number is well under $(N_s + 1)/2$.

The total number of atoms, of course, must remain an integer, and the optical lattice has a finite size. In our examples with $N_s = 4n + 1$ sites and $N_f = 2n + 1$ fermions, the background occupation of $\frac{1}{2}$ makes $2n + \frac{1}{2}$ fermions, and the half of the fermion in the peak adds up to make the correct total fermion number $2n + 1$. If the number of sites is even, the system compensates by putting another soliton at the edge of the lattice, similar to Shockley edge states [44]. If the number of sites is even and the number of fermions precisely half of it, numerically, all solitons may vanish. The zero state is then doubly degenerate, and, as we have not tried to assert any control over the state in the degenerate subspace that gets the last fermion, the numerics decides for us.

The restriction $|a| > |\mu|$ and a and μ exhibiting the opposite signs could be relaxed to read $|a + \mu| < |a - \mu|$. If this condition is violated, the primary soliton, the counterpart of the half-fermion in our examples, emerges at the edge of the lattice, and the possible extra soliton at the center.

III. FERMION NUMBER 1/3

We may also generalize the half-fermion concept to fractionalization to values $1/n$, for any integer n , by considering defects in an n -fold degenerate ground state, analogously to the generalization of the polymer system [18, 41]. To illustrate, we consider the fractional fermion number $1/3$. We consider the ground state with a $1/3$

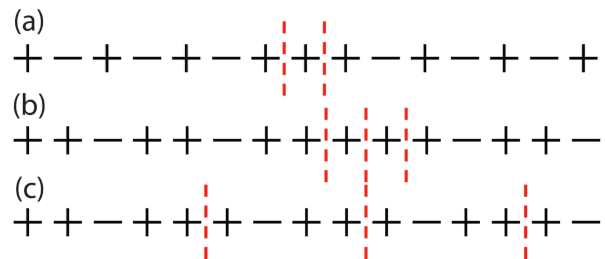


FIG. 7: The nonuniform spatial profile for the hopping amplitudes. (a) Here ‘ \pm ’ denote the couplings $a \pm \mu$ in Eq. (6) where one of the signs of the hopping amplitudes has been changed. Introducing the sign switch generates two defects that are marked by the vertical lines. (b) Here ‘ \pm ’ denote the couplings $a \pm \mu$ in Eq. (42), with $A_k^{(p)}$ given by Eq. (43), where one of the signs in the middle has been switched. In this case the sign change introduces three defects (marked by vertical lines). The first defect represents the boundary between the $p = 0$ and $p = 2$ three-fold degenerate configurations of Eq. (43); the second between $p = 2$ and $p = 1$; and the third between $p = 1$ and $p = 0$. Part (c) represents the same configuration as shown in (b), but with the three defects moved apart.

atomic filling factor. We assume that the hopping amplitude between the lattice sites reads

$$\kappa_k^{(p)} = a + A_k^{(p)} \mu. \quad (42)$$

Here the phase factors $A_k^{(p)}$ exhibit a periodicity of three lattice sites and define a three-fold degenerate ground state (in the limit of an infinite lattice) for the values $p = 0, 1, 2$. We choose

$$A_k^{(p)} = \frac{1}{3} - \frac{4}{3} \cos \left[\frac{4\pi(k+p)}{3} \right]. \quad (43)$$

Then for $p = 0$ we have

$$x + x + x - x + x + x - x + x + x - x \cdots, \quad (44)$$

where we again use an x to denote a lattice site and \pm the couplings $a \pm \mu$. Similarly, for $p = 1$ we obtain

$$x + x - x + x + x - x + x + x - x + x \cdots. \quad (45)$$

In the dimerized lattice system with the coupling (6), one may easily observe that changing the sign of one of the hopping amplitudes corresponds to adding *two* identical defects in the systems [Fig. 7(a)] and by changing the number of atomic states in the vacuum by one (for the ground state of the average of $1/2$ atoms per site). The half fermion results from sharing the extra state evenly between the defects. Similarly, one may show that changing one of the signs of the hopping amplitudes in Eq. (42) corresponds to adding one atomic state in the $1/3$ filled vacuum. It is relatively easy to see that such a sign switch can be viewed as *three* identical defects that join together the three degenerate vacuum configurations of Eq. (43),

representing the boundaries between the $p = 0$ and $p = 2$, $p = 2$ and $p = 1$, as well as the $p = 1$ and $p = 0$ states; see Fig. 7(b-c). If the defects are moved wide apart compared to the size of the kink bound states, the extra atomic state has to be split equally between the defects, resulting in the $1/3$ fermion number.

IV. LOW ENERGY CONTINUUM LIMIT AND FRACTIONALIZATION IN RELATIVISTIC FIELD THEORY

In the continuum limit the Hamiltonian (1) [with $\Omega(\mathbf{r})$ defined in Eqs. (17) and (18)] can be transformed [45, 46, 47] into a relativistic Dirac Hamiltonian exhibiting fractional fermion number in quantum field theory [2]. The transformation is mathematically the same as in the 1D polymer case [3, 18, 45, 46, 47], but the physics is rather different: in our atomic system the kink $\varphi(x)$ appears in the em-induced coupling between the internal atomic states, and not as a physical domain wall kink.

A particular advantage of the continuum quantum field theory is that it is amenable to a simple description. The continuum limit of the low-energy expansion corresponds to the linearization of the band structure about the Fermi surface by writing $\epsilon(p) \simeq \epsilon(p_F) + (p - p_F)\epsilon'(p_F)$, with the Fermi momentum $p_F = \pi/2d$, and keeping only terms to leading order in small d . It becomes accurate in the dilute gas limit, when the atomic correlation length $\xi \simeq |ad/\mu|$, from Eq. (15), is much larger than the lattice spacing. In the continuum limit we write the fermionic annihilation operators for the even and odd sites as continuous functions of the lattice spacing d :

$$c_{2k+1} \equiv (-1)^{(2k+1)/2} \sqrt{2d} u[(2k+1)d], \quad (46)$$

$$c_{2k} \equiv (-1)^k \sqrt{2d} v(2kd). \quad (47)$$

With these identifications, the continuum limit proceeds exactly as in the polymer case [3]. To leading order in small d we obtain

$$u'(2nd) \simeq [u(2nd+d) - u(2nd-d)]/2d, \quad (48)$$

$$v'(2nd+d) \simeq [v(2nd+2d) - v(2nd)]/2d, \quad (49)$$

$$u(2nd) \simeq [u(2nd+d) + u(2nd-d)]/2, \quad (50)$$

$$v(2nd+d) \simeq [v(2nd+2d) + v(2nd)]/2. \quad (51)$$

Here $u'(nd)$ denotes a discrete spatial derivative of u . By setting $\epsilon_k = (-1)^k \delta/2$ and with the hopping determined by Eq. (17), the Hamiltonian (1) reads

$$\begin{aligned} H/\hbar = & -2id^2a \sum_n [u^\dagger(nd)v'(nd) + v^\dagger(nd)u'(nd)] \\ & + \frac{\delta d}{2} \sum_n [u^\dagger(nd)u(nd) - v^\dagger(nd)v(nd)] \\ & + 2i\mu d \sum_n \varphi(nd) [u^\dagger(nd)v(nd) - v^\dagger(nd)u(nd)]. \end{aligned} \quad (52)$$

In the continuum limit we replace $nd \rightarrow x$ and $d \sum_n \rightarrow \int dx$. Combining the two states into a two-component spinor

$$\Psi(x) \equiv \begin{pmatrix} u \\ v \end{pmatrix} \quad (53)$$

and making the transformation: $\Psi \rightarrow \exp(i\pi\sigma^3/4)\Psi$, we may express Eq. (52) as the relativistic (1+1)-dimensional Dirac Hamiltonian [2, 3] for the spinor $\Psi(x)$ coupled to a bosonic condensate $\varphi(x)$,

$$H = \int dx [c\hbar\Psi^\dagger\sigma^2\frac{d\Psi}{dx} + \hbar g\varphi\Psi^\dagger\sigma^1\Psi + mc^2\Psi^\dagger\sigma^3\Psi]. \quad (54)$$

Here we have identified $c = 2da$, $g = 2\mu$, and $m = \hbar\delta/(8d^2a^2)$. The σ^i denote the Pauli spin matrices, g the coupling coefficient, m the fermionic mass, and c the speed of light. In the atomic system the spinor components refer to the two internal atomic levels. The corresponding eigenvalue system reads

$$\begin{aligned} \left(c\hbar\frac{d}{dx} + \hbar g\varphi \right) u(x) - mc^2v(x) &= Ev(x), \\ \left(-c\hbar\frac{d}{dx} + \hbar g\varphi \right) v(x) + mc^2u(x) &= Eu(x). \end{aligned} \quad (55)$$

Note that in the relativistic Dirac equation (55) for the fermionic atoms both the speed of light and the coupling coefficient may be controlled by the different em field amplitudes a and μ . The mass of the Dirac fermions vanishes at the exact resonance coupling between the two atomic levels and is linearly proportional to the detuning that can be accurately changed in the experiments. Moreover, in the relativistic theory, as in our atomic scheme, the bosonic field $\varphi(x)$ can be taken to be a static classical background field. Thus, the atomic Hamiltonian (1) with a defect in the pattern of alternating hopping amplitudes [Eq. (18)] can also be written in the continuum limit in the form (54) and (55).

Fractionalization in the relativistic theory is described as follows [2, 3]. Suppose the bosonic field φ in Eq. (54) has a doubly-degenerate ground state, for example arising from a double-well potential $V(\varphi) \propto (\varphi^2 - \gamma^2)^2$. There are two minima, $\varphi(x) = \pm\gamma$, and the reflection symmetry $\varphi \leftrightarrow -\varphi$ is spontaneously broken. Consequently there are topological solitons $\varphi(x)$ (also known as ‘‘kinks’’) interpolating between these two degenerate minima. For weak coupling, we make a Born-Oppenheimer approximation, so that the fermion number must now be defined through the second quantization of the fermion field in the presence of this background soliton. Being a Dirac particle, the fermion has both positive and negative energy single-particle eigenstates, and therefore an associated Dirac negative energy sea in which the negative energy states are occupied. This Dirac sea is the ultimate physical origin of the fractional fermion number [4].

The second-quantized number operator can be defined in two equivalent ways. The formal relativistic quantum field theory definition is [48]

$$N \equiv \frac{1}{2} \int dx [\Psi^\dagger(x), \Psi(x)], \quad (56)$$

with the commutator ensuring that the fermion particle number vanishes in the free vacuum. Equivalently, one defines the physical particle number in the soliton sector as being measured *relative to* the free vacuum sector, so that the fermion number density is

$$\rho(x) = \int_{-\infty}^{0^-} dE (|\Psi_E(x)|^2 - |\psi_E(x)|^2) \quad (57)$$

where Ψ_E (ψ_E) are the fermion single-particle energy eigenstates in the soliton (free) vacuum sector. Once again, by construction the fermion particle number vanishes in the free vacuum.

It is easiest to exhibit the fermion number fractionalization when $m = 0$ in the Dirac Hamiltonian (54). In this case the Hamiltonian has a conjugation symmetry that pairs positive and negative energy states. For every eigenvalue ϵ of Eq. (55) there exists an eigenvalue $-\epsilon$, and the corresponding eigenfunctions are paired according to $\Psi_{-\epsilon} = \sigma^3 \Psi_\epsilon^*$. However, the nontrivial feature of this fermion-soliton system is that there is also a zero-energy bound state $\Psi_0(x)$, and furthermore, this state is localized at the soliton jump:

$$\Psi_0(x) = \left(A \exp \left[-\frac{g}{c} \int_0^x dy \varphi(y) \right] \right). \quad (58)$$

This state is self-conjugate, $\sigma^3 \Psi_0 = \Psi_0$, and results in a doubly-degenerate soliton sector vacuum [2].

Thus, the mode expansion of the second quantized fermion field operator has the form

$$\Psi(x, t) = a \Psi_0(x) + \int dk \left(e^{-iE_k t} b_k \Psi_{E_k}(x) + e^{iE_k t} c_k^\dagger \Psi_{E_k}^*(x) \right) \quad (59)$$

where b_k and c_k denote annihilation operators for continuum fermion and antifermion modes (respectively), while the operator a is the annihilation operator for the self-conjugate zero-energy state. Then the fermion number operator (56) in the presence of the soliton reads [3]:

$$N = \frac{1}{2} [a^\dagger, a] + \frac{1}{2} \int dk \left([b_k^\dagger, b_k] + [c_k, c_k^\dagger] \right) = a^\dagger a - \frac{1}{2} + \int dk (b_k^\dagger b_k - c_k^\dagger c_k), \quad (60)$$

Note that the operators a and a^\dagger couple the two degenerate fermion-soliton ground states in which the zero energy single-particle state is either occupied or not. Thus, it follows from (60) that the ground-state fermion-soliton states possess fractional fermion numbers $\pm 1/2$.

The same conclusion is reached [4] using the subtracted definition (57) of the number density operator, if we simply combine the expression (57) with the completeness of the two sets of eigenstates, $\{\Psi_E\}$ and $\{\psi_E\}$, in the soliton and vacuum sector, respectively:

$$\int_{-\infty}^{0^-} dE |\Psi_E(x)|^2 + |\Psi_0(x)|^2 + \int_{0^+}^{+\infty} dE |\Psi_E(x)|^2 = \int_{-\infty}^{+\infty} dE |\psi_E(x)|^2 \quad (61)$$

Thus, in the fermion-soliton vacuum defined with only negative energy states filled (i.e., with the zero mode empty), the fermion number density (57) is

$$\rho(x) = -\frac{1}{2} |\Psi_0(x)|^2 \quad (62)$$

which yields fermion number $-1/2$. Similarly, if the zero energy state is filled, the fermion number is $+1/2$, consistent with the result above from (60).

In fact, it is not just the expectation value of the fermion number that is half-integer; with a suitable physical definition of the number density operator as a smeared operator defined over a physical sampling region, it can also be shown that these half-integer values are *eigenvalues* of the number operator [42, 43]. The fermion-soliton system yields *eigenstates* of this physical number operator. Furthermore, the fractional part of the fermion number has a topological character: it is insensitive to local deformations of the bosonic soliton field, depending only on its asymptotic behavior [3].

For $m \neq 0$, the situation becomes even more interesting [13]. In this case, the conjugation symmetry of the Dirac Hamiltonian (54) is broken and the positive and negative energy states are no longer paired in a simple way. In the limit of a slowly varying soliton (on the scale of the fermion Compton wavelength), the soliton acts as an inhomogeneous electric field that polarizes the Dirac sea vacuum, thereby building up local fermion number at the location of the kink. A straightforward one-loop computation [13, 49, 50] yields a fermion number taking arbitrary fractional values:

$$N = -\frac{1}{\pi} \arctan \left(\frac{\hbar g \gamma}{m c^2} \right) \quad (63)$$

In our atomic system studied in Section IIB, we studied the conjugation symmetric case where $\epsilon_k = 0$ in Eq. (24), which corresponds to the conjugation symmetric $m = 0$ case in the continuum limit. If instead we set a nonvanishing effective detuning δ for the hopping field between the two atomic levels, so that $\epsilon_k = (-1)^k \delta/2$ with $\delta \neq 0$, the symmetry between the valence and the conduction band states is broken, and they are no longer coupled together in a simple way. In the continuum limit this corresponds to the $m \neq 0$ case in which the conjugation symmetry is broken. Then the fractional part of the

fermion number may exhibit any value, in the continuum limit according to

$$N = -\frac{1}{\pi} \arctan\left(\frac{4\mu}{\delta}\right). \quad (64)$$

The ratio $4\mu/\delta$ between the coupling strength and the effective detuning therefore determines the fractional part of the particle number. In experiments this could be engineered accurately, allowing a potentially controlled way of preparing the fractional part of the eigenvalues by tuning the mass of the Dirac fermions.

An interesting further variation would be to study the temperature dependence of the fermion number. The above discussion is all for zero temperature, but at nonzero temperature the fermion number may develop nontopological contributions [14] and the fluctuations may become nonvanishing [15], depending on the form of the kink. Nonetheless, the fractional fermion is not a singular feature of the theory at $T = 0$ that vanishes without a trace at any nonzero temperature. As a concrete example, for a kink the finite temperature induced fermion number is [14, 15, 51, 52, 53]

$$\langle N \rangle_T = -\frac{2}{\pi} \sum_{n=0}^{\infty} \frac{y^2 \sin \theta}{((2n+1)^2 + y^2) \sqrt{(2n+1)^2 \cos^2 \theta + y^2}}$$

where $\theta = \arctan(4\mu/\delta)$, and $y = mc^2/(\pi T)$. This expression smoothly reduces to the zero temperature result (64) as $T \rightarrow 0$. The fluctuations $(\Delta N)^2 \equiv \langle N^2 \rangle - \langle N \rangle^2$ also has a characteristic temperature dependence [15].

The crucial part of our proposal for fractional particle number is the em field $\varphi(x)$ in Eq. (18). This is very different from the fermion particle number fractionalization in polymers, as our fermionic fields are not coupled to a bosonic matter field with a domain-wall soliton. Instead, the coherent em field with a topologically appropriate phase profile is coupled to the FD atoms via internal transitions. This results in the quantization of the FD atomic gas with nontrivial topological quantum numbers corresponding to the soliton sector of the relativistic 1+1 quantum field theory models of fractionalization. On the other hand, a spatially constant phase profile $\varphi(x)$ represents the FD vacuum sector exhibiting integer particle numbers.

V. OPTICAL DETECTION

The dimerized optical lattice resulting from the alternating pattern of the hopping matrix elements causes the single-particle density of states to acquire an energy gap, which in the limit $N_s \rightarrow \infty$ equals $4\hbar|\mu|$; see Eq. (14). The zero state is located at the center of the gap. The resulting excitations at half the gap energy could be detected by resonance spectroscopy [54]. This provides indirect evidence of fractionalization, as in the polymer systems [18]. Because in our scheme [1] the gap is proportional to the amplitude of the em field inducing the

hopping, the size of the energy gap can be controlled experimentally.

Such mid-gap spectroscopy, however, would not provide information about fermion numbers. In this section we consider direct optical measurements of the expectation value and of the fluctuations of the fermion number in order to ascertain if they are compatible with fractionalization.

We assume that far off-resonant light excites the atoms, and consider the 1D optical lattice to be optically thin. We take the light scatterer at each lattice site to be much smaller than the wavelength of the detection light. In the case of off-resonant excitation the amplitude of the light scattered from an essentially point source is proportional to the number of atoms [25]. Also, for off-resonant excitation the scattering is coherent; the scattered light has a fixed phase relation to the incoming light, and is fully capable of interference. Thus, in a given point of observation the positive frequency parts of the field operator for the light scattered from the lattice sites simply sum up to

$$\hat{E}^+ = C \sum_k \alpha_k c_k^\dagger c_k. \quad (65)$$

C is a constant containing the overall intensity scale of the detection light. The factors α_k include aspects such as intensity and phase profiles of the detection light, effects of the spin state at each site k on light-atom coupling, and changes of the amplitude and phase of the light as it propagates from the lattice sites to the point of observation. A more detailed description how Eq. (65) is obtained can be found in Ref. [25].

A. Measuring atom numbers

In forward scattering and variations thereof such as phase contrast imaging, the scattered and the incoming light interfere. The ultimate measurement of the intensity in effect records the expectation value of the scattered electric field $E = \langle \hat{E}^+ \rangle$. The observable at the detector is

$$E = \sum_k \alpha_k \langle c_k^\dagger c_k \rangle = \sum_{kp} \alpha_k U_{kp}^2 n_p. \quad (66)$$

This is a linear combination of the expectation values of the numbers of fermions at each lattice site with the coefficients α_k , exactly as introduced in Eq. (34).

We now construct a numerical example about forward scattering as a means to detect the fractional fermion. We make use of the fact that the fermion species at the alternating lattice sites are likely to be different. We assume that the detection light is far blue-detuned in one species and far red-detuned in the other, and that the two dipole matrix elements are comparable. One may then find a laser tuning such that the intensity of the scattered light is the same for both species. However, the lights

scattered by the two species are out of phase by π , and out of phase with the incident light by $\pm\pi/2$. With the usual tricks of phase contrast imaging, the relative phase of incident and scattered light is then adjusted so that in interference the light from one species directly adds to the incident light, and the light from the other species subtracts. We incorporate the alternating sign into the definition of our observable, and write

$$E = \sum_k \alpha_k (-1)^k \langle c_k^\dagger c_k \rangle. \quad (67)$$

We take it that the incoming light is a plane wave with a constant phase and amplitude. It will therefore just contribute a common constant into the envelope factors α_k , hence α_k basically stands for the amplitude of the light as transmitted through the imaging system from the source point, lattice site \mathbf{r}_k , to the observation point, \mathbf{r} . We adopt a rudimentary physical-optics model according to which an imaging lens first takes a Fourier transform of the light field at the object plane, passes only the Fourier components that make it through the aperture of the lens, and then takes another Fourier transform to form the image.

Let us say that the geometry has been arranged in such a way that all Fourier components of light in the plane of the aperture up to the absolute value K are passed, the rest are blocked. Depending on where the object and image planes are, there might be a scaling of the image with respect to the source, but we ignore both this and the usual inversion of the image with respect to the object. The transfer function of the lens from point \mathbf{r}_k to the point \mathbf{r} , normalized to the peak value of unity, is then $2J_1(K|\mathbf{r} - \mathbf{r}_k|)/(K|\mathbf{r} - \mathbf{r}_k|)$, and so we have the transmitted field

$$E(\mathbf{r}) = \sum_k (-1)^k \langle c_k^\dagger c_k \rangle \frac{2J_1(K|\mathbf{r} - \mathbf{r}_k|)}{K|\mathbf{r} - \mathbf{r}_k|}. \quad (68)$$

We present an example in Fig. 8. We choose the parameters $\mu = -0.1a$, and the numbers of sites and fermions $N_s = 129$ and $N_f = 65$. Given the imaging light with the wavelength λ , we use the cutoff wave number $K = 2\pi/(\sqrt{5}\lambda)$. This would be appropriate, for instance, if the imaging system had the numerical aperture $F = 1$ and the lattice resided near the focal plane of the imaging lens; or if the numerical aperture were the rather extreme $F = 0.5$, and both the optical lattice and its image were removed by two focal lengths from the lens. We assume that the wavelength of the lattice light and of the imaging light are the same and that the spacing between the lattice sites is $d = \lambda/4$. Under these circumstances it would difficult to resolve individual lattice sites. In practice a 1D optical lattice can be significantly stretched by changing the intersection angle between the laser beams, and so the resolution of the optical detection is not necessarily limited by the lattice site spacing even if the wavelengths of the lattice light and the light used for optical detection were comparable.

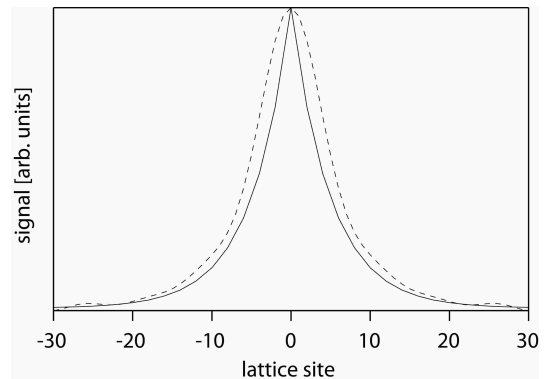


FIG. 8: Optical image (dashed line) of the half-fermion density profile on top of a uniform background density with the average number of 0.5 atoms per lattice site produced by a specific imaging system, as discussed in the text. The density profile (solid line) that is being imaged is also shown. The size of the soliton is set by the choices $N_s = 129$, $N_f = 65$, and $\mu = -0.1a$, corresponding to the correlation length of $\xi \simeq 10$ lattice sites.

We set $d = \lambda/4$ simply to limit the number of parameters to consider. We plot the optically imaged fermion lattice along the line of the atoms (dashed line), and the number of fermionic atoms in excess of the average occupation number $\frac{1}{2}$ for the even-numbered sites that carry the lump with $\langle \tilde{N} \rangle = \frac{1}{2}$ (solid line) as obtained from Eq. (34). The curves are normalized so that the maxima overlap.

Although the quantum operator \hat{E}^+ describing the phase contrast imaging is not directly proportional to the fermion number operator \tilde{N} defined by Eq. (34), its expectation value produced by the imaging system, Eq. (68), nevertheless accurately depicts a resolution rounded version of the half-fermion lump. In fact, phase contrast imaging has been used for nondestructive monitoring of a Bose-Einstein condensate [55], and the absorption of a single trapped ion has been detected experimentally long ago [56]. While a lot of assumptions went into our specific example, a light scattering experiment along these lines should be feasible with the technology available today.

B. Measuring atom number fluctuations

1. Intensity of Bragg peaks

In the absence of interference with the incoming light, the straightforward observable is the intensity of the light scattered from the atoms. We have

$$I = \langle \hat{E}^- \hat{E}^+ \rangle. \quad (69)$$

With illumination of the optical lattice by a focused laser beam it is possible to arrange the field strength of the detection light vary from site to site approximately as a Gaussian. Let us further assume, contrary to the

previous section, that the atoms at the lattice sites are identical as far as light scattering is considered. If now the detection is carried out in the direction of constructive interference (Bragg scattering) so that the light amplitudes scattered from the lattice sites have the same phase, and far enough from the lattice so that the propagation distance of light from each lattice site to the detector is approximately the same, the field strength is of the form

$$\hat{E}^+ = \sum_k e^{-(k/w)^2} c_k^\dagger c_k. \quad (70)$$

A measurement of the intensity of the light therefore measures the square of the atom number operator, $I = \langle \hat{N}^\dagger \hat{N} \rangle = |\langle \hat{N} \rangle|^2 + (\Delta N)^2$, as in Eq. (37), with the Gaussian weights α_k^G .

The key point in the detection of the correlated atom number fluctuations responsible for the half-fermion is to measure the coherent fluctuations (37), i.e., to rely on interference of light scattered from different lattice sites. If the light scattered from individual sites can be resolved or if a too broad angular average in the detection or other such cause wipes out the interferences $[\alpha_k^* \alpha_l \rightarrow \delta_{kl} \alpha_k^* \alpha_k]$, the scattered light probes the “incoherent” fluctuations $(\Delta N)_i$ [Eq. (41)], as if the fermion number fluctuations in each site were independent.

The problem in detecting the fractional fermion number is that in the measured signal of the light intensity the fluctuations ΔN appear on a nonzero background. We demonstrate by plotting in Fig. 9 separately the contribution $|\langle \hat{N} \rangle|^2$, as if the fermion numbers were precisely fixed, and the fluctuation term $(\Delta N)^2$. We also show the fluctuations $(\Delta N)_i^2$ that would result if the fermion number fluctuations at adjacent sites were uncorrelated. These are given as functions of the width of the focus w of the laser beam. Here $N_s = 129$, $N_f = 65$, and we choose $\mu = -0.9a$ to make a sharply localized zero state.

In our discussion we employ the Gaussian width $w = 4$, which would ordinarily represent very tight focusing. Here the contribution from atom number fluctuations to light intensity is two orders of magnitude below the coherent intensity, whereas the fluctuations from uncorrelated fermion numbers would make a contribution an order magnitude smaller than the coherent intensity. As our detection light was assumed to be far off resonance, photon number fluctuations are Poissonian. Under otherwise ideal conditions, including absolute knowledge and control of all experimental parameters pertaining to intensity of the scattered light, the detection of about a hundred photons could reveal the difference between correlated and uncorrelated fermion numbers, whereas a quantitative study of the actual correlated fermion number requires the detection of about 10,000 photons. Unfortunately, a large number of scattered photons means a large number of recoil kicks on the fermions. Currently available optical lattices likely cannot absorb the assault of hundreds of photon recoils without developing some

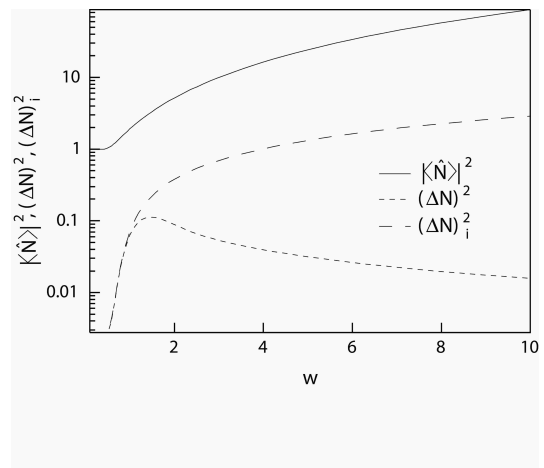


FIG. 9: The intensity of light scattered from the optical lattice if the fermion numbers did not fluctuate, $|\langle \hat{N} \rangle|^2$, and the additional intensity due to fermion number fluctuations $(\Delta N)^2$, as a function of the size of the focus w of the driving light given in the lattice units. We also display the added intensity $(\Delta N)_i^2$ that would result if fermion number fluctuations were uncorrelated between adjacent lattice sites. The soliton parameters are $N_s = 129$, $N_f = 65$, $\mu = -0.9a$.

form of a dynamics that complicates the phenomena we are analyzing.

2. Variations of intensity measurements

While the scattered light in principle conveys information about the fluctuations of atom number, the method to extract the information we have discussed so far is quite challenging.

A way to discard the uniform background of $\frac{1}{2}$ fermions per lattice site, as in going from operator \hat{N} to \tilde{N} in Eq. (34), would be most useful. One might, for instance, think of the alternating-sign Gaussian envelope α_k^A , as defined in Eq. (40) and (in principle) realized as discussed in Sec. V A, and still look in the direction of ordinary Bragg scattering. By virtue of the first form of Eq. (36), the coherent signal $|\langle \hat{N} \rangle|^2$ from the background of $\frac{1}{2}$ indeed cancels in the limit of a broad envelope. However, the fluctuation part $(\Delta N)^2$ as appropriate for α_k^A is not small, and does not directly bear witness to the small fluctuations of the atom number of the half-fermion. On the contrary, as discussed in Sec. II B 2, in this case the fluctuations of the atom number under the Gaussian envelope are larger than one would expect if the atom number fluctuations at adjacent sites were uncorrelated.

A scheme that fares better is based on the observation that off-resonant light scattering is coherent. If the atom numbers were fixed, the field scattered by the lattice as a whole were also completely coherent with the incoming light. One could then tap part of the incident light and impose a suitable attenuation and phase on it so that on the detector the incident light exactly cancels the scat-

tered light. Given the fluctuating atom numbers, it is correspondingly possible in principle to arrange things so that the detected intensity originates entirely from atom number fluctuations.

In technical terms, assume that the incident and scattered fields are superimposed on the detector so that the electric field operator is

$$\hat{E}^+ = C \sum_k \alpha_k (c_k^\dagger c_k - \langle c_k^\dagger c_k \rangle) \quad (71)$$

instead of Eq. (65). This eliminates the coherent part of the intensity $\propto |\langle \hat{N} \rangle|^2$, leaving only the fluctuation part $(\Delta N)^2$ in Eq. (37). The situation of Eq. (71) may be realized operationally by minimizing the detected intensity with adjustments of the attenuation and the phase of the canceling light. The remaining intensity is then directly proportional to the the square of atom number fluctuations under the envelope of the detection light. A reduction in the minimum detected intensity with an increasing size of the focus of the driving light would be a signature of anomalous atom number fluctuations characteristic of the fractional fermion. Another approach to eliminate the coherent part of the light intensity is to exploit the diffraction pattern of the scattered light from the regular array of the lattice sites and detect the photon number fluctuations at the location of the destructive interference of the coherent $\propto |\langle \hat{N} \rangle|^2$ contribution of the scattered light.

Although our goal here is not a specific experimental design, another variation with potential to overcome the accumulation of atom recoil merits a mention. So far we have dealt with what in essence is spontaneous Bragg scattering. Recently, induced Bragg scattering has been introduced as a method to study the condensates in detail [57, 58]. In optical lattices the strong spatial confinement may complicate the Bragg spectroscopy measurements [59, 60], but the advantage of the light-stimulated Bragg scattering is that conceivably the light pulses could be made so short that the harmful effects of photon recoil do not have time to build up during the measurement.

VI. CONCLUDING REMARKS

The optical lattice could be part of a larger harmonic trap, which may also affect the energy profile ϵ_k in the

Hamiltonian (1). The length scale over which the energy variation due to the trap becomes comparable to the energy gap is then $r_0 \equiv (8\hbar|\mu|/M\omega^2)^{1/2}$, where ω denotes the trap frequency and M the mass of the atom. For the system to have a locally homogeneous gap value, this length scale should be much larger than the correlation length ξ . Moreover, in order to have a better experimental control over the atom numbers and to maintain the one-half filling throughout the lattice, we require that the energy gap is nonvanishing everywhere, or $r_0 \gtrsim N_h d$. The nonvanishing gap parameter and the locally homogeneous limit could therefore be reached with a sufficiently weak trap and by experimentally controlling the size of the gap. By using sufficiently large values of $|\mu|$, it might also be possible to study the effective zero temperature limit $|\mu| \gg k_B T/\hbar$ and to have a better control over the light scattering measurements. Finally, the sharp edges of the optical lattice system with hard-wall boundaries could be prepared, e.g., by shining blue-detuned laser beams at the lattice ends.

We could possibly also construct complex higher dimensional models in 2D or 3D optical lattices with atoms coupled to nontrivial em fields. In relativistic (2+1)D quantum field theory, a fermionic field coupled to a bosonic field exhibiting a vortex profile results in fermion particle number fractionalization [3, 61, 62, 63, 64]. It may also be possible to find analogies to relativistic (3+1)D quantum field theoretical models [2], e.g., by using em field superpositions to prepare topologically nontrivial atomic configurations [39, 40, 65, 66, 67, 68]. The significance of localized zero energy modes in fermionic systems has also recently been discussed in the context of quantum teleportation [69], using results from the quantum field theoretical analysis in [70].

Acknowledgments

This work was financially supported by the EPSRC, the DFG, the U.S. DOE., the U.S. NSF, and NASA. GD thanks the University of Adelaide and the ITP in Heidelberg for hospitality and support while on sabbatical.

-
- [1] J. Ruostekoski, G. V. Dunne, and J. Javanainen, Phys. Rev. Lett. **88**, 180401 (2002).
 - [2] R. Jackiw and C. Rebbi, Phys. Rev. D **13**, 3398 (1976).
 - [3] For a review, see: A. Niemi and G. Semenoff, Phys. Reports **135**, 99 (1986), and references therein.
 - [4] R. Jackiw, Dirac Prize Lecture, hep-th/9903255.
 - [5] J. Javanainen and J. Ruostekoski, Phys. Rev. Lett. **91**, 150404 (2003).
 - [6] D. Jaksch and P. Zoller, New J. Phys. **5**, 56 (2003).
 - [7] E.J. Mueller, Phys. Rev. A **70** 041603 (2004).
 - [8] K. Osterloh, M. Baig, L. Santos, P. Zoller, and M. Lewenstein, Phys. Rev. Lett. **95**, 010403 (2005).
 - [9] K.S. Novoselov, A.K. Geim, S.V. Morozov, D. Jiang, M.I. Katsnelson, I.V. Grigorieva, S.V. Dubonos, and A.A. Firsov, Nature (London) **438**, 197 (2005).
 - [10] Y. Zhang, Y.-W. Tan, H.L. Stormer, and P. Kim, Nature

- (London) **438**, 201 (2005).
- [11] M.I. Katsnelson, K.S. Novoselov, and A.K. Geim, *Nature Phys.* **2**, 620 (2006).
- [12] An atomic system in a hexagonal lattice, analogous to graphene was addressed by S.-L. Zhu, B. Wang, and L.-M. Duan, *Phys. Rev. Lett.* **98**, 260402 (2007).
- [13] J. Goldstone and F. Wilczek, *Phys. Rev. Lett.* **47**, 986 (1981).
- [14] I. J. R. Aitchison and G. V. Dunne, *Phys. Rev. Lett.* **86**, 1690 (2001).
- [15] G. V. Dunne and K. Rao, *Phys. Rev. D* **64**, 025003 (2001).
- [16] P.W. Anderson, *Phys. Today* **50**, 42 (October 1997).
- [17] W.P. Su, J.R. Schrieffer, and A.J. Heeger, *Phys. Rev. Lett.* **42**, 1698 (1979); *Phys. Rev. B* **22**, 2099 (1980).
- [18] A.J. Heeger, S. Kivelson, J.R. Schrieffer, and W.P. Su, *Rev. Mod. Phys.* **60**, 781 (1988).
- [19] R. B. Laughlin, H. Störmer and D. Tsui, *Rev. Mod. Phys.* **71**, 863 (1999).
- [20] R. de-Picciotto, M. Reznikov, M. Heiblum, V. Umansky, G. Bunin, and D. Mahalu, *Nature* **389**, 162 (1997).
- [21] L. Saminadayar, D.C. Glattli, Y. Jin, and B. Etienne, *Phys. Rev. Lett.* **79**, 2526 (1997).
- [22] V.J. Goldman and B. Su, *Science* **267**, 1010 (1995).
- [23] F.E. Camino, W. Zhou, and V.J. Goldman, *Phys. Rev. B* **72** 075342 (2005).
- [24] O. Morice, Y. Castin, and J. Dalibard, *Phys. Rev. A* **51**, 3896 (1995); J. Ruostekoski and J. Javanainen, *Phys. Rev. Lett.* **82**, 4741 (1999); J. Ruostekoski, *Phys. Rev. A* **60**, R1775 (1999); **61**, 033605 (2000); Z. Idziaszek, K. Rzazewski, and M. Lewenstein, *Phys. Rev. A* **61**, 053608 (2000).
- [25] J. Javanainen and J. Ruostekoski, *Phys. Rev. A* **52**, 3033 (1995).
- [26] J. Ruostekoski and D.F. Walls, *Phys. Rev. A* **56**, 2996 (1997).
- [27] J. Ruostekoski, M.J. Collett, R. Graham, and D.F. Walls, *Phys. Rev. A* **57**, 511 (1998).
- [28] N.R. Cooper, N.K. Wilkin, and J.M.F. Gunn, *Phys. Rev. Lett.* **87**, 120405 (2001).
- [29] I.B. Mekhov, C. Maschler, and H. Ritsch, *Phys. Rev. Lett.* **98**, 100402 (2007).
- [30] The optical cavity transmission spectra was analyzed by I.B. Mekhov, C. Maschler, and H. Ritsch, *Nature Phys.* **3**, 319 (2007).
- [31] M. Raizen, C. Salomon, and Q. Niu, *Phys. Today* **50**, 30 (1997).
- [32] B. Paredes, A. Widera, V. Murg, O. Mandel, S. Fölling, I. Cirac, G.V. Shlyapnikov, T.W. Hänsch, and I. Bloch, *Nature* **429**, 277 (2004).
- [33] C.D. Fertig, K.M. O'Hara, J.H. Huckans, S.L. Rolston, W.D. Phillips, and J.V. Porto, *Phys. Rev. Lett.* **94**, 120403 (2005).
- [34] D. Jaksch, C. Bruder, J.I. Cirac, C.W. Gardiner, and P. Zoller, *Phys. Rev. Lett.* **81**, 3108 (1998).
- [35] O. Mandel, M. Greiner, A. Widera, T. Rom, T.W. Hänsch, and I. Bloch, *Nature* **425**, 937 (2003).
- [36] A.B. Deb, G. Smirne, R.M. Godun, and C.J. Foot, e-print arXiv:0705.1258.
- [37] We have here redefined some signs of the variables used in Ref. [5] in order to simplify the overall notation.
- [38] J. Leach, M.R. Dennis, J. Courtial, and M.J. Padgett, *Nature* **432**, 165 (2004).
- [39] J. Ruostekoski and J.R. Anglin, *Phys. Rev. Lett.* **86**, 3934 (2001).
- [40] J. Ruostekoski and Z. Dutton, *Phys. Rev. A* **72**, 063626 (2005).
- [41] J.R. Schrieffer, in *Highlights of Condensed Matter Theory: Proceedings of the International School of Physics Enrico Fermi*, Course LXXXIX (1983), ed. by F. Bassani (Elsevier, New York), Vol. 89, p. 300.
- [42] J.S. Bell and R. Rajaraman, *Phys. Lett. B* **116**, 151 (1982); *Nucl. Phys. B* **220**, 1 (1983).
- [43] S. Kivelson and J. R. Schrieffer, *Phys. Rev. B* **25**, 6447 (1982); R. Jackiw, A.K. Kerman, I. Klebanov, and G. Semenoff, *Nucl. Phys. B* **225**, 233 (1983).
- [44] W. Shockley, *Phys. Rev.* **56**, 317 (1939).
- [45] R. Jackiw and G.W. Semenoff, *Phys. Rev. Lett.* **50**, 439 (1983).
- [46] H. Takayama, Y. R. Lin-Liu and K. Maki, *Phys. Rev. B* **21**, 2388 (1980).
- [47] B. Horowitz and J. A. Krumhansl, *Sol. State Comm.* **26**, 81 (1978).
- [48] J. D. Bjorken and S. Drell, *Relativistic Quantum Fields* (McGraw-Hill, New York, 1965).
- [49] F. Wilczek, "Adiabatic Methods in Field Theory", in 1984 TASI Lectures in Elementary Particle Physics, Ann Arbor, edited by D. Williams.
- [50] R. MacKenzie and F. Wilczek, *Phys. Rev. D* **30**, 2194 (1984), *Phys. Rev. D* **30**, 2260 (1984).
- [51] A. J. Niemi and G. W. Semenoff, *Phys. Lett. B* **135**, 121 (1984).
- [52] V. Soni and G. Baskaran, *Phys. Rev. Lett.* **53**, 523 (1984).
- [53] C. Coriano and R. R. Parwani, *Phys. Lett. B* **363**, 71 (1995) [arXiv:hep-th/9506211]; A. S. Goldhaber, R. Parwani and H. Singh, *Phys. Lett. B* **386**, 207 (1996) [arXiv:hep-th/9605163].
- [54] In a finite-size lattice the midgap mode may also exist in the vacuum state. However, this is always spatially separated from the soliton bound state.
- [55] M.R. Andrews, M.O. Mewes, N.J. van Druten, D.S. Durfee, D.M. Kurn, and W. Ketterle, *Science* **273**, 84 (1996).
- [56] D. J. Wineland, W. M. Itano and J. C. Bergquist, *Opt. Lett.* **12**, 389 (1987).
- [57] D.M. Stamper-Kurn, A.P. Chikkatur, A. Görlitz, S. Inouye, S. Gupta, D.E. Pritchard, and W. Ketterle, *Phys. Rev. Lett.* **83**, 2876 (1999); J. Steinhauer, N. Katz, R. Ozeri, N. Davidson, C. Tozzo, F. Dalfovo, *Phys. Rev. Lett.* **90**, 060404 (2003).
- [58] M. Saba, T.A. Pasquini, C. Sanner, Y. Shin, W. Ketterle, and D.E. Pritchard, *Science* **307**, 1945 (2005).
- [59] T. Stöferle, H. Moritz, C. Schori, M. Köhl, and T. Esslinger, *Phys. Rev. Lett.* **92**, 130403 (2004).
- [60] X. Du, S. Wan, E. Yesilada, C. Ryu, D.J. Heinzen, Z.X. Liang, and Biao Wu, e-print arXiv:0704.2623.
- [61] G. W. Semenoff, *Phys. Rev. Lett.* **53**, 2449 (1984).
- [62] F. D. M. Haldane, *Phys. Rev. Lett.* **61**, 2015 (1988).
- [63] R. R. Parwani and A. S. Goldhaber, *Nucl. Phys. B* **359**, 483 (1991).
- [64] E. G. Flekkoy and J. M. Leinaas, *Int. J. Mod. Phys. A* **6**, 5327 (1991).
- [65] H.T.C. Stoof, E. Vliegen, and U. Al Khawaja, *Phys. Rev. Lett.* **87**, 120407 (2001).
- [66] J. Ruostekoski and J.R. Anglin, *Phys. Rev. Lett.* **91** 190402 (2003).
- [67] C.M. Savage and J. Ruostekoski, *Phys. Rev. Lett.* **91**, 010403 (2003).

- [68] J. Ruseckas, G. Juzeliunas, P. Öhberg, and M. Fleischhauer, Phys. Rev. Lett. **95**, 010404 (2005).
- [69] G. W. Semenoff and P. Sodano, arXiv:cond-mat/0605147.
- [70] A. J. Niemi and G. W. Semenoff, Phys. Rev. D **30**, 809 (1984).